THE COMPARISON OF PERFORMANCE OF THE MENTER SHEAR STRESS TRANSPORT AND BALDWIN-LOMAX TURBULENCE MODELS WITH RESPECT TO CFD PREDICTION OF LOSSES IN HP AXIAL TURBINE STAGES

Piotr Lampart, Jerzy Świrydczuk, Andrzej Gardzilewicz
Institute of Fluid Flow Machinery
Polish Academy of Sciences, Gdańsk, Poland
e-mail: lampart@imppan.imp.pg.gda.pl

Sergey Yershov, Andrey Rusanov
Institute of Mechanical Engineering Problems
Ukrainian Academy of Sciences, Kharkov, Ukraine
e-mail: yershov@ipmach.kharkov.ua

ABSTRACT

A series of computations with a 3D RANS solver FlowER are made to compare the performance of the Menter shear stress transport and Baldwin-Lomax turbulence models in predicting flow patterns and losses in HP axial flow steam turbines. Two HP stator-rotor stages are computed - one whose flow by turbomachinery standards can be referred to as regular, and another with flow separation at the root. The comparison of computations using the Menter SST and Baldwin-Lomax turbulence models exhibits differences as far as the trailing edge losses, development of secondary flows and separations, and the resulting prediction of span-wise distributions of losses. However, the tendency is that for the same relatively refined grid resolutions, the level of pitch/span averaged losses for the Menter SST turbulence model is only slightly above that of Baldwin-Lomax. The computational results are validated on a model stator/rotor air turbine, giving a comparison of span-wise distributions of velocity and swirl angle downstream of the rotor trailing edge and a comparison of efficiency characteristics for three operational regimes of the model turbine.

INTRODUCTION

Simulation of turbulent effects is of great importance for the computation of 3D viscous compressible turbomachinery flows. There are a number of turbulence models ranging from algebraic eddy-viscosity to differential Reynolds stress models. None of them has been reported so far to correctly describe all types of flows. Therefore, it is crucial that a chosen model should be appropriate for the investigated flow and easy to implement without considerably increasing computational costs. The simplest turbulence model is an algebraic two-layer eddy-viscosity model of Baldwin-Lomax 1974 that has become a standard for turbomachinery codes. Its great assets are easy numerical implementation, relatively good numerical stability, reasonable performance in wall regions, and low CPU costs. A disadvantage is that the model performs poorer in adverse pressure gradient boundary layers and free shear flows away from body surfaces, and does not account for effects of inlet free-stream turbulence.

Two-equation models are also very often developed as closures of RANS solvers. There are a variety of k-ε models, including those of Jones & Launder 1973, Launder & Sharma 1974 or Chien 1982. k-ε models are known to perform relatively well in free shear layer flows. On the other hand, they require a number of damping functions near the walls, and even with damping functions they are unable to predict well velocity profiles and skin friction in high-Reynolds number flows.

Unlike k-ε models, a series of k-ω models, see Wilcox 1988, Chima 1996, do not need damping functions near the wall and allow a simple Dirichlet condition to be specified there. Truly inconsistent here, an asymptotic behaviour of ω as it approaches the wall is usually replaced by a finite value, as the molecular viscosity in the boundary layer exceeds the eddy-viscosity and the form of turbulence here does not necessarily have an effect on the mean velocity profiles and skin friction. The k-ω model of Wilcox is also capable of treating rough walls and surface mass injections, and is also superior to the k-ε in compressible flows. Another model of Wilcox 1994 contains extra functions to improve the transition. One drawback of the k-ω models is their excessive sensitivity to the free-stream value of ω, a deficiency not featuring in the k-ε approach.

An idea put forward by Menter 1994 is to combine good features of both k-ω and k-ε models, at the same time eliminat-

ing their deficiencies. This is pronounced in his new model called the baseline model (BSL) where k-ω model is activated in the near wall region, and then switched to the k-ε model in the wake region and free shear layers. The formulation of the standard high-Reynolds number k-ε model is transformed to a k-ω formulation. It is then multiplied by sides by a blending function (1-F_1) and added to an original formulation of the k-ω model multiplied by F_1, with the blending function F_1 changing from *1* in the logarithmic region of the boundary layer gradually to *0* in the wake region.

Departing from this model, Menter 1994 also proposed another model he refers to as the shear stress transport model (SST), modifying the eddy viscosity so as to account for the effects of turbulent shear stress transport. The idea is based on Bradshaw's experimental observations that the principal turbulent shear stress is proportional to the turbulent kinetic energy in the wake region of the boundary layer. Arguing that superior performance of the k-ω model in the logarithmic region of the boundary layer has a limited effect on the eddy viscosity in the wake region which finally determines the ability of an eddy-viscosity model to predict strong adverse pressure gradient flows, and referring to the results of the model of Johnson & King 1985 that enforces the Bradshaw's observation and shows an improvement over standard algebraic models by reducing the wake region eddy viscosity in adverse pressure gradient flows, Menter redefines the eddy viscosity into the following form: $\nu_t = a_1 k / \max(a_1\omega, \Omega F_2)$, where a_1 is a Bradshaw constant, Ω-vorticity (absolute value) and F_2 is a function that changes from *1* in boundary layer flows to *0* for free shear layers. Due to the fact that in adverse pressure gradient boundary layers the production of turbulent kinetic energy is larger than its dissipation, the above formulation guarantees the proportional relationship between the principal turbulent shear stress and the turbulent kinetic energy in the boundary layer ($\tau = \nu_t \Omega = \rho a_1 k$).

Differential or algebraic Reynolds stress models form a great potential to improve predictions from RANS solvers. However, numerical implementation or numerical stability is still an unresolved question here, also in classical test cases, not only with respect to complex turbomachinery geometries. Therefore, software developers still tend to hold on to simple but robust algebraic or two-equation eddy-viscosity models and improve them for particular applications. This tendency is also preserved in development of a code FlowER - RANS solver of 3D viscous compressible flows in axial and radial turbomachinery shortly described below, see Yershov & Rusanov 1996ab, Yershov et al. 1999, 2000. A comprehensive review of turbulence modelling for CFD can be found e.g. in a book of Wilcox 1993, paper of Menter 1996 and dissertation of Larsson 1996.

Previous works of the authors, Yershov et al. 2001, indicate that the Menter SST model has an upper hand over the Baldwin-Lomax model in modelling transonic compressor flows, for example ROTOR 37. For this case, it turned out to be impossible to compute over the entire range of operation of the compressor using the Baldwin-Lomax model, whereas the Menter SST model yielded a very good agreement between the experimental and computational results, including the total pressure ratio and adiabatic efficiency over the entire operational range of the compressor. The work of Lampart et al. 2001, concerning the flow analysis in 3D single-row model cascades reveal that the Menter SST model gives a better resolution of exit total pressure loss contours, and better agreement in span-wise distribution of exit velocity and exit angle, including the overturning and underturning due to secondary flows. The aim of the present paper is to test the performance of the two-equation eddy-viscosity shear stress transport model of Menter, superior in the authors' opinion between the two-equation models, as compared to that of the modified algebraic eddy-viscosity model of Baldwin-Lomax, in the context of predicting flow patterns and efficiency characteristics for HP stages of real large power steam turbines.

3D RANS SOLVER

Basic equations

3D flow of viscous and compressible gas through a turbine stage can be described by a set of unsteady Reynolds-averaged Navier-Stokes equations written in a curvilinear body-fitted coordinate system (ξ, η, ζ), rotating with an angular speed ϖ (the computational domain extends on blade-to-blade passages, axial gaps and radial gaps above/below unshrouded blade tips)

$$\frac{\partial QJ}{\partial t} + \frac{\partial\left(E\xi_x + F\xi_y + G\xi_z\right)J}{\partial \xi} + \frac{\partial\left(E\eta_x + F\eta_y + G\eta_z\right)J}{\partial \eta} + \frac{\partial\left(E\zeta_x + F\zeta_y + G\zeta_z\right)J}{\partial \zeta} = HJ, \qquad (1)$$

where:
$$Q = \begin{bmatrix} \rho \\ \rho u \\ \rho v \\ \rho w \\ h \end{bmatrix}; \quad H = \begin{bmatrix} 0 \\ 2\rho v\varpi + \rho\varpi^2 r_x \\ -2\rho u\varpi + \rho\varpi^2 r_y \\ 0 \\ 0 \end{bmatrix};$$

$$E = \begin{bmatrix} \rho u \\ \rho u^2 + p - \tau_{xx} \\ \rho uv - \tau_{xy} \\ \rho uw - \tau_{xz} \\ (h+p)u - u\tau_{xx} - v\tau_{xy} - w\tau_{xz} + q_x \end{bmatrix};$$

$$F = \begin{bmatrix} \rho v \\ \rho uv - \tau_{xy} \\ \rho v^2 + p - \tau_{yy} \\ \rho vw - \tau_{yz} \\ (h+p)v - u\tau_{xy} - v\tau_{yy} - w\tau_{yz} + q_y \end{bmatrix};$$

$$G = \begin{bmatrix} \rho w \\ \rho uw - \tau_{xz} \\ \rho vw - \tau_{yz} \\ \rho w^2 + p - \tau_{zz} \\ (h+p)w - u\tau_{xz} - v\tau_{yz} - w\tau_{zz} + q_z \end{bmatrix};$$

where $h = \frac{1}{\gamma - 1}\frac{p}{\rho} + \frac{u^2 + v^2 + w^2 - \varpi^2 r^2}{2} + const$,

$$\tau_{ij} = \tau_{mij} + \tau_{tij}; \quad \tau_{m_{ij}} = 2\mu_m\left(S_{ij} - S_{nn}\delta_{ij}/3\right);$$

$$\tau_{t_{ij}} = 2\mu_t\left(S_{ij} - S_{nn}\delta_{ij}/3\right) - 2\rho k\delta_{ij}/3; \quad q = -\lambda\nabla T .$$

The symbols p, ρ, u, v, w represent the pressure, density and components of the velocity, while τ_{mij}, τ_{tij}, τ_{ij} are molecular, turbulent and total viscous stress, S_{ij} - mean strain-rate tensor; T – temperature; μ=(μ_m,+μ_t) - effective (molecular+ turbulent) viscosity, q – heat flux, $\lambda = \lambda_m + \lambda_t = c_p(\mu_m / Pr_m + \mu_t / Pr_t)$ – effective (molecular + turbulent) heat conductivity, Pr_m,, Pr_t – molecular and turbulent Prandtl numbers. The turbulence effects are modelled using two eddy-viscosity models - an algebraic model of Baldwin-Lomax and two-equation model of shear stress transport (SST) proposed by Menter.

Baldwin-Lomax turbulence model

In the original Baldwin-Lomax model the boundary layer is divided into two domains - an inner and outer layer. The turbulent viscosity in the inner region is calculated from the Prandtl concept of mixing length

$$\mu_{turb} = \mu^i_{turb} = \rho l^2 \Omega ; \qquad (2)$$

where Ω is the vorticity (absolute value), l - mixing length

$$l = ky\left[1 - \exp\left(-y^+ / A^+\right)\right]; \quad y^+ = y\sqrt{\rho_w / \tau_w} / \mu_w ,$$

where y is a distance from the wall, τ_w - wall shear stress, k=0.41 (Karman constant), A^+ = 26 (van Driest constant),.

The turbulent viscosity in the outer region of the boundary layer is defined by the modified Clauser formula

$$\mu_{turb} = \mu^0_{turb} = \alpha C_{CP} \rho F_{WK} F_k \ , \qquad (3)$$

where $\alpha = K_{CL}\frac{1.55}{1+\varphi}$, K_{CL} = 0.0168 (Clauser const.), C_{CP} =1.6,

$\varphi = 0.55\left[1 - \exp\left(-0.243\sqrt{z} - 0.298\, z\right)\right]$, z=Re_0/425 - 1, $\mathrm{Re}_\theta = \frac{\rho U \theta}{\mu}$

F_{WK} is the wake function

$$F_{WK} = \min(\eta_{\max} F_{\max}, C_{WK} y_{\max} U_D^2 / F_{\max}),$$

where U_D=U_{max}-U_{min} is a difference between the maximum and minimum velocity at the boundary layer section; C_{WK} = 0.25 (wake constant), F_{max} and y_{max} are found from the maximum of the function

$$F(y) = y\Omega\left[1 - \exp\left(y^+ / A^+\right)\right] .$$

F_K is the Klebanoff intermittency factor

$$F_k = \left[1 + 5.5\left(C_k y / y_{\max}\right)^6\right]^{-1},$$

where C_k = *0.3* (Klebanoff constant). The division between the inner and outer layer is set at a point nearest to the wall where

$$\mu^i_{turb} = \mu^0_{turb} .$$

The flow is assumed turbulent if at some point of the boundary layer profile the eddy viscosity calculated as prescribed above is 14 time larger than the molecular viscosity of undisturbed flow. Otherwise, the boundary layer is thought to be laminar at this section.

The original model of Baldwin-Lomax in the code FlowER is modified by Yershov & Rusanov 1997 to improve its calculation of eddy viscosity in the regions of separation and wake.

For separated flows, the velocity U_{min} is assumed as a negative of the maximum backflow velocity. The coefficient C_{WK} in the recirculation zone is increased according to the formula of Kinsey & Eastep 1988

$$C_{WK} = C^{BL}_{WK}\left(1 + D_W y_{sep} / L\right) ,$$

where C^{BL}_{WK} is the wake constant in the original Baldwin-Lomax model; y_{sep} - backflow thickness; L - characteristic dimension (blade span for endwall boundary layers or pitch for boundary layers at blade walls), $D_W \approx 50$. After Colantuoni et al. 1989, in the proximity of separation and reattachment the wall shear stress is calculated as a distance-averaged value

$$\bar{\tau}_w = \frac{1}{L(\xi)}\int_0^L \tau_w(\xi)\, d\xi, ,$$

where ξ is the curvilinear body-fitted coordinate, L - is a distance along the wall. In order to assure smooth changes of turbulent viscosity, the flow history is taken into account using a simple relaxation procedure that refers to turbulent viscosity upstream, see Fletcher 1988

$$\mu_{t_i} = (1 - \chi)\tilde{\mu}_{t_i} + \chi\mu_{t_{i-1}} .$$

where μ_{t_i}, $\tilde{\mu}_{t_i}$, $\mu_{t_{i-1}}$ are the resultant turbulent viscosity, its preliminary value and turbulent viscosity one cell upstream, respectively, and χ=0.1-0.3 is the correlation coefficient.

For wakes, the Clauser formula is improved and reduced

$$\mu_{CL} = \max_{y}(\mu_{te})\widetilde{F}_K ,$$

where μ_{te} is the turbulent viscosity at the trailing edge,

$$\widetilde{F}_k = \left[1 + 5.5\left(y/\widetilde{\delta}\right)^6\right]^{-1}, \ \widetilde{\delta} = \min(y_{\max}/C_k, 2\delta_\omega),$$

and δ_ω is a cross-wake distance between the wake axis and a point in the wake where the vorticity assumes a maximum value. The relation $\widetilde{\delta} \approx 2\delta_\omega$ is usually valid. The wake axis is determined as a line that consists of points where the velocity is minimal and the entropy function reaches its maximum. For a near wake the following relaxation formula is applied, see Rodi & Srinivas 1989

$$\mu_{turb} = \mu_{CL} + (\mu_{te} - \mu_{CL})\ exp[-\xi/(20\delta_{te})],$$

where μ_{CL}, μ_{te}, μ_{turb} are coefficients of turbulent viscosity calculated in the wake from the Clauser formula, calculated at the trailing edge from the Baldwin-Lomax model, and the resultant turbulent viscosity in the near wake, respectively; ξ is the distance from the trailing edge section and δ_{te} is the trailing edge boundary layer thickness.

As the original Baldwin-Lomax model was put forward for 2D flow simulation, its implementation in 3D requires a procedure to account for intersecting effects of different walls and regions (endwalls and blade walls; wake, tip leakage). The resultant turbulent viscosity is calculated as an average of turbulent viscosities calculated with respect to different walls (regions) for independent length scales, weighted with the distance to the other wall (region). The details of the procedure are described in Yershov & Rusanov 1997, Yershov et al. 1999.

Shear stress transport model of Menter

The set of equations in a k-ω formulation reads as below

$$\frac{\partial U}{\partial t} + \frac{\partial R_i}{\partial x_i} = G - D + L; \qquad (4)$$

where: $G = \begin{bmatrix} \tau_{ij}S_{ij} \\ \gamma\ \dfrac{\omega}{k}\tau_{ij}S_{ij} \end{bmatrix}$; $R_i = \begin{bmatrix} \rho k - (\mu + \sigma_k \mu_t)\dfrac{\partial k}{\partial x_i} \\ \rho\omega - (\mu + \sigma_\omega \mu_t)\dfrac{\partial \omega}{\partial x_i} \end{bmatrix}$;

$U = \begin{bmatrix} \rho k \\ \rho\omega \end{bmatrix}$; $D = \begin{bmatrix} \beta^* \rho\omega k \\ \beta\rho\omega^2 \end{bmatrix}$; $L = \begin{bmatrix} 0 \\ 2(1-F_1)\dfrac{\rho\sigma_{\omega 2}}{\omega}\dfrac{\partial k}{\partial x_i}\dfrac{\partial \omega}{\partial x_i} \end{bmatrix}$;

where k is the turbulent kinetic energy; $\omega = \varepsilon/k\beta^*$ – specific dissipation rate, and the turbulent viscosity has the form

$$\mu_t = \frac{\rho k/\omega}{\max[1; \Omega F_2/(a_1\omega)]}.$$

The blending functions F_1 (assuring smooth transition from the k-ω at the wall to the k-ε in free shear layers) and F_2 (assuring the proportional relationship between the principal turbulent shear stress and the turbulent kinetic energy in the boundary layer) have the form

$$F_1 = \tanh\left\{\left[\min\left(A_1; A_2\right)\right]^4\right\}; \ A_1 = \max\left(B_1; B_2\right); \ A_2 = \frac{4\rho\sigma_{\omega 2}k}{CD_{k\omega}y^2};$$

$$F_2 = \tanh\left\{\left[\max\left(2B_1; B_2\right)\right]^2\right\}; \ B_1 = \frac{\sqrt{k}}{\beta^*\omega y}; \ B_2 = \frac{500\mu}{\rho y^2 \omega},$$

$$CD_{k\omega} = \max\left(2\frac{\rho\sigma_{\omega 2}}{\omega}\frac{\partial k}{\partial x_i}\frac{\partial \omega}{\partial x_i}; 10^{-20}\right).$$

A vector of constants $\phi = [\sigma_k, \sigma_\omega, \beta, \gamma]$ in the baseline or shear stress transport models can be written as $\phi = F_1\phi_1 + (1-F_1)\phi_2$, where ϕ_1 is this vector in the k-ω model, and ϕ_2 in the k-ε model written in k-ω formulation. The constants of the SST model assume the following values

$a_1 = 0{,}31$; $\sigma_{k1} = 0{,}85$; $\sigma_{k2} = 1{,}0$; $\sigma_{\omega 1} = 0{,}5$; $\sigma_{\omega 2} = 0{,}856$;

$\beta^* = 0{,}09$; $\beta_1 = 0{,}075$; $\beta_2 = 0{,}0828$; $\gamma_1 = 0{,}553$; $\gamma_2 = 0{,}44$.

Boundary conditions

The boundary conditions for the set of Eqs. (1) are:
- at the walls - no-slip and no heat flux;
- at the inlet - span-wise distribution of the total pressure, total temperature and flow angles at the inlet to the stage;
- at the exit - static pressure (either its span-wise distribution or a value at the mid-span with the radial equilibrium equation).

For the set of Eqs. (4), we have the boundary conditions:
- at the walls:

$$k = 0; \qquad \omega = \frac{60\mu_w}{\rho_w \beta y^2};$$

- at the inlet:

$$k = \frac{3}{2}\left(Tu \cdot U_\infty\right)^2; \qquad \omega = \sqrt{\frac{\max\left(S\Omega, \Omega^2\right)}{\beta^*}}, \ S = \sqrt{\frac{1}{2}S_{ij}S_{ij}},$$

where Tu - inlet free-stream turbulence level;
- at the outlet: values of k and ω are extrapolated from the preceding cell centres.

The computations are carried out in one blade-to-blade passage of the stator and rotor, and converge to a steady state with the condition of spatial periodicity and mixing plane approach assumed. The concept of mixing plane draws on pitch-wise averaging of flow parameters in the axial gap between the stator and rotor. Tip and root leakage flows are not included. The assumed inlet/exit boundary conditions impose the pressure drop and let the mass flow rate be resultant. Comparative calcula-

tions are performed for the same pressure drop across the stage.

Numerical scheme

The governing equations are solved numerically based on cell-centred finite-volume discretisation, Godunov-type upwind differencing, high resolution ENO scheme, and implicit operator δ of Beam & Warming, see Yershov et al. 1999.

VALIDATION OF THE CODE AND TURBULENCE MODELS ON A MODEL AIR TURBINE STAGE (MAT)

The considered model air turbine stage of the Institute of Thermal Engineering (ITC) £ódŸ, Poland - model TK9-TW3, see Wiechowski 1988, has a geometry typical for HP steam turbine stages. It operates with short-height cylindrical blading and aft-loaded stator profiles of aspect ratios: span/chord - 0.73 (stator) and 2.20 (rotor), pitch/chord - 0.86 (stator) and 0.80 (rotor) , span/diameter - 0.08 (stator and rotor). The thermodynamic conditions are: the pressure drop from 1 to 0.9 bar, inlet temperature - 320K, average reaction - 0.23 (nominal conditions), mass flow rate - 4.0 kg/s (nominal conditions). The turbine stage was tested experimentally by Wiechowski 1985 over a wide range of operating conditions u/c_{0T} between 0.3 and 0.9 (u - rotor speed at the mid-span, c_{0T} - theoretical enthalpy drop across the stage), achieved by changing the rotor rotational speed. The available experimental data do not show field contours but disclose, among others, the stage efficiency as well as span-wise distributions of the exit velocity and swirl angle for the stator and rotor in the tested range of operating conditions. Therefore, these quantities will be sought for in the process of computations of the model TK9-TW3 to validate the code and the considered models of turbulence.

The computations are carried out for three values of u/c_{0T} equal to 0.45, 0.54 (nominal conditions) and 0.65. The specific heat ratio and gas constant for the air are assumed as γ=1.401 and R=283 J/(kgK). An H-type grid of 1 200 000 cells (stator + rotor) refined near the endwalls, blade walls, trailing and leading edges is assumed for the computations. Gridding of the flow domain in the meridional view and in the blade-to-blade section is presented in Fig. 1. The results may not be exactly grid-independent, but show little change compared to those of 1 000 000 or 800 000 cells. The total pressure profile at the inlet is assumed uniform, with the inlet endwall boundary layers of thickness 2% of the blade span each, and low inlet free-stream turbulence level.

Fig. 2 shows the comparison of computational results, obtained with the help of the Baldwin-Lomax and Menter SST models of turbulence, with experimental data for the absolute velocity and absolute swirl angle (measured from the direction normal to the cascade front) at the exit from the rotor for u/c_{0T}=0.45, 0.54 and 0.65. The computed distributions were captured at the section located 135% of the axial chord downstream of the rotor trailing edge, that is at a distance corresponding to the location of the measuring probe at the experimental facility. In general, the computational and experimental results reveal satisfactory qualitative and also quantitative agreement for the three investigated values of load, however, the distributions and their span-wise averaged values obtained with the help of the Menter SST closure seem to agree better with the experimental results than those of the Baldwin-Lomax turbulence model. The reference axial section is relatively far downstream of the blading system, therefore, it is expected that the processes of mixing and dissipation of 3D flow structures are largely accomplished there. This is why the experimental distributions of the investigated quantities do not exhibit considerable 3D peaks characteristic for sections more upstream. Neither do the computational curves for the Menter SST model, which suggests the appropriate rate of dissipation of 3D flows in this model. The span-wise locations of those largely dissipated peaks and other non-uniformities of distributions are reproduced relatively well. The curves are less „smooth" for the Baldwin-Lomax model, with 3D peaks more clear, which suggests too little dissipation of flow non-uniformities. It seems that the Menter SST model better predicts the level of eddy viscosity in flow, and rate of dissipation of flow non-uniformities.

The computed efficiency characteristics of the stage as a function of load u/c_{0T} obtained with the considered two closures of RANS equations are shown in Fig. 3 against the experimental graph. The stage efficiency is defined here as the stage loss with the exit energy subtracted from unity, see also Appendix. For the three examined operating conditions the Baldwin-Lomax model overestimates the stage efficiency, while the Menter SST model apparently underestimates it, but still leaving room for better accuracy (and higher efficiency) on more refined grids. The differences in estimation of the stage efficiency between the two models are below 1%.

In the next chapter, we will concentrate on differences in global characteristics as well as in local flow patterns in turbine flows modelled with the help of the Baldwin-Lomax and Menter SST models. Two HP stages of a real large power turbine will be computed. These stages operate at the same pressure drop of 0.9 as the model air turbine, and have similar aspect ratios (short-height blading) and the same stator and rotor profiles, however differing in profile chords, stagger angles and blade numbers. The flow in the first HPT stage can, by turbomachinery standards, be referred to as regular and well-tailored to the flow conditions. Regular flow patterns in the second HPT stage are disturbed by the separation at the rotor root. The separation is a result of inadequate local incidence on the rotor blade at the root, and can relatively easy be corrected in the design process by more careful stator/rotor matching for the assumed operational range of thermodynamic parameters. However, the example provides a fertile field for investigations of the effect of turbulence modelling on computational flow patterns and characteristics, as in the case of adverse pressure gradient flows, including separated flows, the performance of the Baldwin-Lomax model is usually poor and it is expected that the Menter SST model should produce more adequate results.

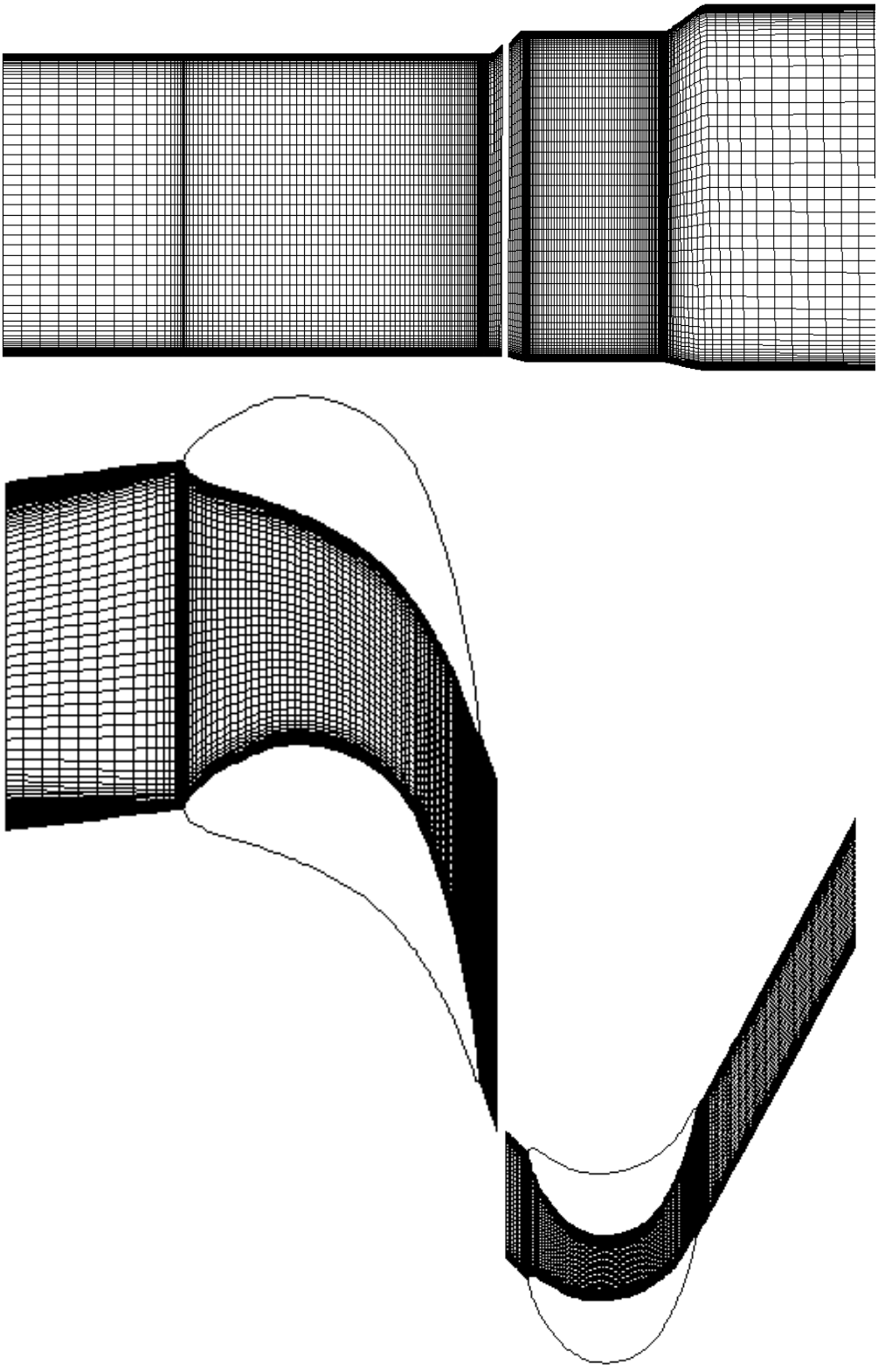

Fig. 1. MAT - computational grids for the stator and rotor cascades of the model turbine stage in meridional view (top) and in the blade-to-blade section at the mid-span (bottom).

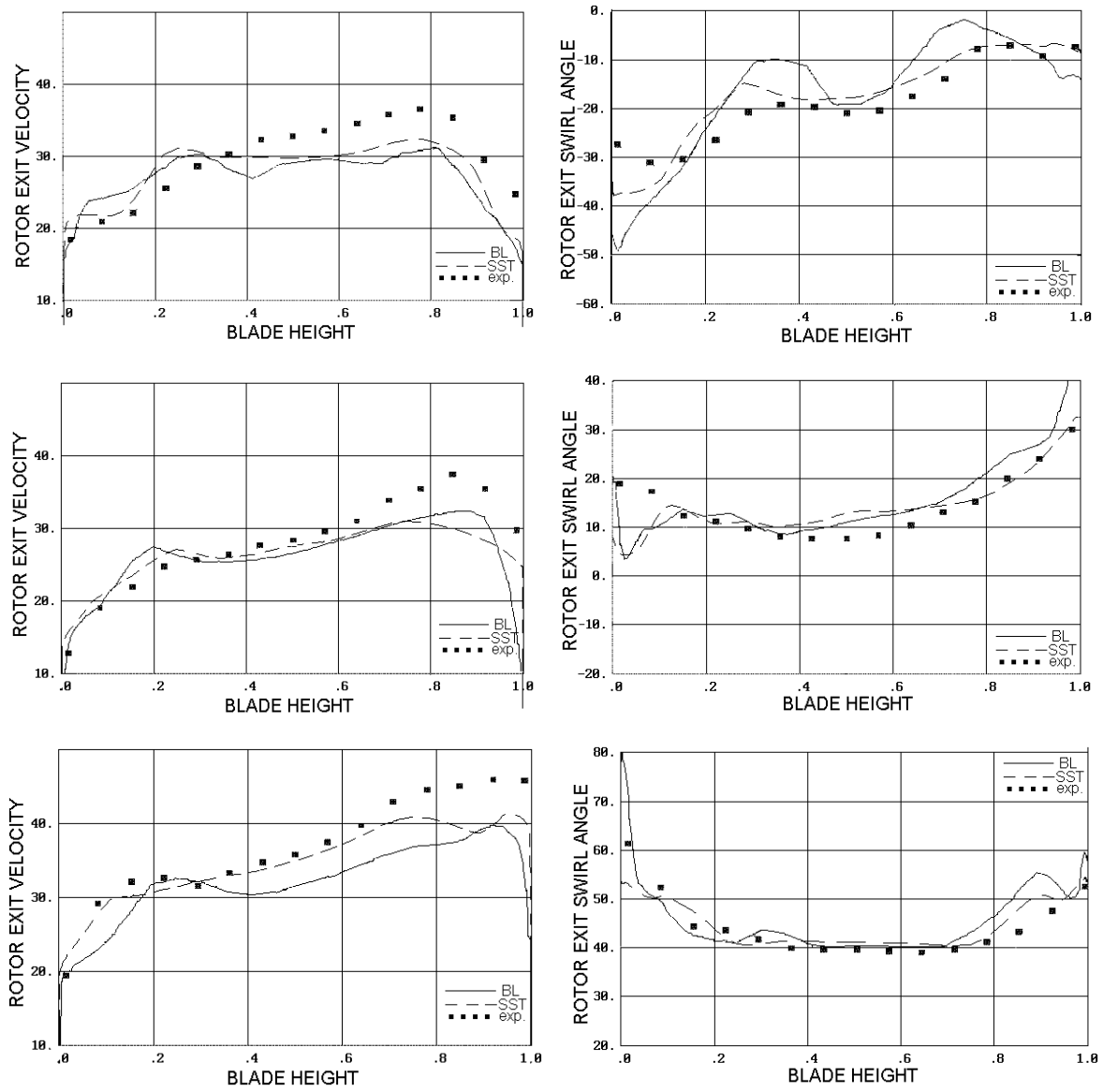

Fig. 2. MAT - computed (BL and SST) and experimental, absolute velocity (left) and absolute swirl angle (right) at the exit from the rotor for u/c_{0T}=0.45 (top), 0.54 (centre) and 0.65 (bottom).

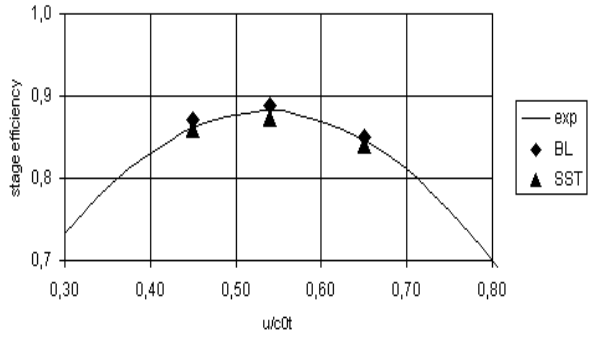

Fig. 3. MAT - computed and experimental efficiency characteristics of the model air turbine stage as a function of load u/c_{0T}.

HP TURBINE STAGE (HPT1)

The HP stage of a large power steam turbine to be tested first is a typical impulse stage with short-height cylindrical blading, including aft-loaded stator profiles, operating at the pressure drop from 96 to 88 bar, inlet temperature - 780K, flow rate - 155 kg/s, stator exit Mach number - 0.32, average reaction - 0.25. The aspect ratios are: span/chord - 0.57 (stator) and 1.59 (rotor), pitch/chord - 0.57 (stator) and 0.78 (rotor), span/diameter - 0.059 (stator) and 0.064 (rotor). The specific heat ratio and gas constant are assumed as γ=1.29 and R=426 J/(kgK). The calculations are carried out on an H-type grid of 960 000 cells (stator + rotor) refined near the endwalls, blade walls, trailing and leading edges. Similar to the model air turbine, the total pressure profile at the inlet is assumed uniform, with the inlet endwall boundary layers of thickness 2% of the blade span each, and low inlet free-stream turbulence level.

Fig. 4 shows the comparison of total pressure contours downstream of the stator trailing edge obtained with Baldwin-Lomax and Menter SST turbulence modelling. The figures do not particularly differ, save for the fact that the wake is slightly thicker and the total pressure peaks due to secondary flows, especially that at the tip, are closer to the endwalls in the case of the Menter SST model. Velocity vectors at the suction surface of the rotor presented in Fig. 5 indicate an earlier onset, in terms of the stream-wise coordinate, and a larger span-wise extension of the secondary flow zones in the Baldwin-Lomax model. Fig. 6 showing the comparison of contours of the entropy function ($s=p/\rho^{\gamma}$, p - pressure, ρ - density) in the rotor at

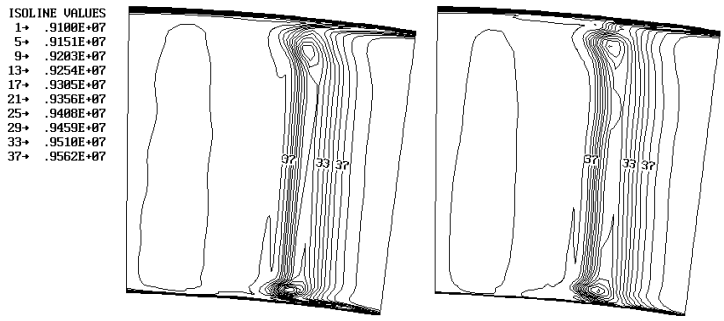

Fig. 4. HPT1 - total pressure contours downstream of the stator; Baldwin-Lomax (left), Menter SST (right).

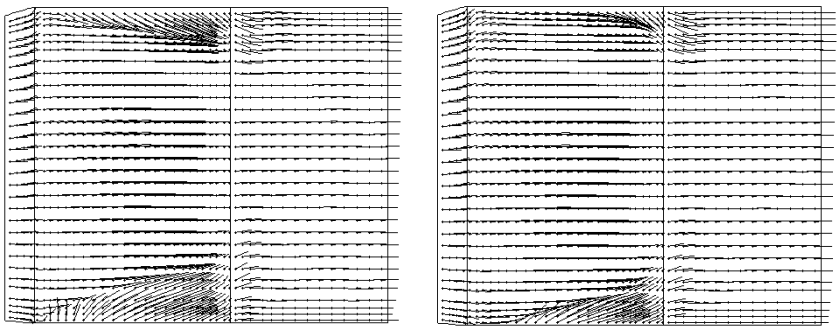

Fig. 5. HPT1 - velocity vectors at the suction surface of the rotor; Baldwin-Lomax (left), Menter SST (right).

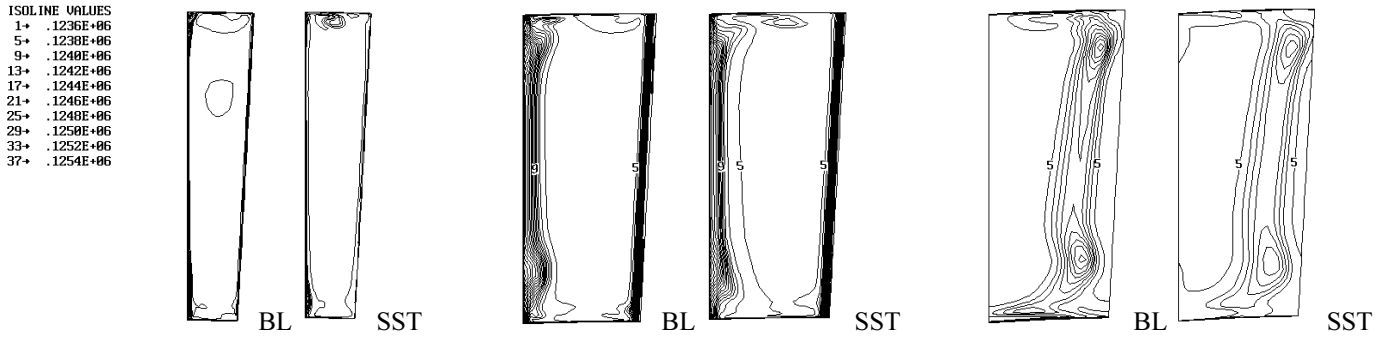

Fig. 6. HPT1 - entropy function contours in the rotor: 75% axial chord downstream of the leading edge (left), at the trailing edge (centre) and 18% axial chord downstream of the trailing edge (right); Baldwin-Lomax (left), Menter SST (right).

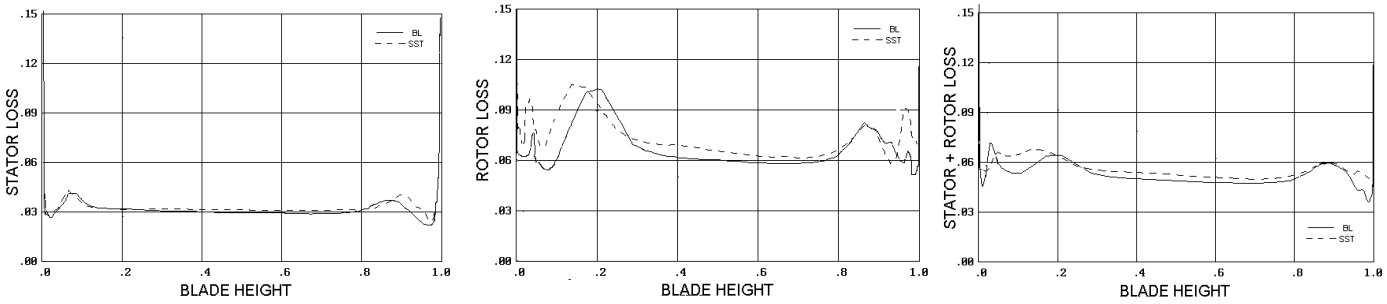

Fig. 7. HPT1 - span-wise distribution of kinetic energy losses in the stator (left), rotor (centre) and stage without exit energy (right).

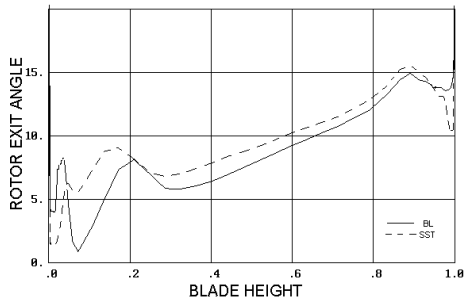

Fig. 8. HPT1 - span-wise distribution of rotor exit swirl angle.

streamwise-subsequent sections illustrates the development of secondary flow patterns in the rotor, confirming the tendency observed in the stator that the loss centres due to secondary flows remain closer to the endwalls, and the wake and boundary layers are slightly thicker in the case of the Menter SST model.

Fig. 7 shows a span-wise distribution of kinetic energy losses in the stator, rotor and stage without the exit energy, see also the definitions of losses given in Appendix. The stator loss is captured in the axial gap 10% of the stator axial chord downstream of the trailing edge, the rotor loss - 45% of the rotor axial chord downstream of the trailing edge. The tendency is that the Menter SST model predicts a slightly higher level of 2D losses. For the stator, the difference is about 0.2%, for the rotor - 0.4%. However, the similar distributions at the trailing edges of the stator and rotor will show that the boundary layer losses obtained using the Menter SST and Baldwin-Lomax are nearly the same, below a 0.1% accuracy margin, both for the stator and rotor. The main difference in predictions of the 2D loss is in the level of the trailing edge loss due to the fact that the Menter SST model predicts more eddy viscosity in the wake, resulting is a larger rate of dissipation of kinetic energy. The Menter SST model predicts also more eddy viscosity in the region of secondary flows, and a higher local loss. However, the difference in the level of secondary loss is decreased due to a smaller span-wise extension of the secondary flow zone predicted by the Menter SST model. The secondary loss maxima are also relocated compared to those of the Baldwin-Lomax model. The pitch/span averaged value of the stator loss differs by 0.2% (BL - 3.9%, SST - 4.1%), the rotor loss - 0.5% (BL - 6.6%, SST - 7.1%). The tendencies observed for the stator and rotor summarised on the graph of stage losses without the exit energy, captured similar to that of the rotor loss, that is 45% of the rotor axial chord downstream of the rotor trailing edge. It is clear that the Menter SST curves have the 2D loss base slightly moved up and 3D peaks increased and relocated, compared to those of the Baldwin-Lomax model. Due to the low reaction of the stage and a resulting small contribution of the rotor loss to the overall stage loss, the pitch/span averaged values of the sta-ge loss without the exit energy differ by 0.3% only (BL - 5.2%, SST - 5.5%). The mean exit swirl angle differs by 1.1° (BL - 9°, SST - 10.1°). The exit angle peaks due to 3D effects undergo moderate changes in position and magnitude, see Fig. 8. For the same pressure drop, both turbulence models predict similar resultant mass flow rates (BL - 155 kg/s, SST - 154.5 kg/s).

HP TURBINE STAGE (HPT2)

The second HP stage of another large power steam turbine is a similar impulse stage, operating at the pressure drop from 79 to 71 bar, inlet temperature - 760K, flow rate - 165 kg/s, stator exit Mach number - 0.35, average reaction - 0.20. The aspect ratios are: span/chord - 0.81 (stator) and 2.14 (rotor), pitch/chord - 0.73 (stator) and 0.75 (rotor), span/diameter - 0.069 (stator) and 0.073 (rotor). HPT2 has the same stator and rotor profiles as MAT and HPT1, but differing in chords and stagger angles (also blade number is different). Perfect gas constants are assumed as γ=1.29, R=428 J/(kgK). The calculations are also made on an H-type grid of 960 000 cells (stator + rotor).

The comparison of total pressure contours downstream of the stator trailing edge presented in Fig. 9 confirms the observations from Fig. 4. The wake is slightly thicker and the total pressure peaks due to secondary flows, especially that at the tip, are closer to the endwalls in the case of the Menter SST model. Velocity vectors at the suction surface of the rotor presented in Fig. 10 again indicate an earlier onset and larger span-wise extension of the secondary flow zones in the Baldwin-Lomax model. A separation from the suction surface at the root also comes into play here. This phenomenon is also clear from Fig. 11 showing entropy function contours in the rotor 6% of the blade span from the root. The separation in the Menter SST model is clearly delayed and the pitch-wise extension of the separation zone reduced, compared to the predictions of the

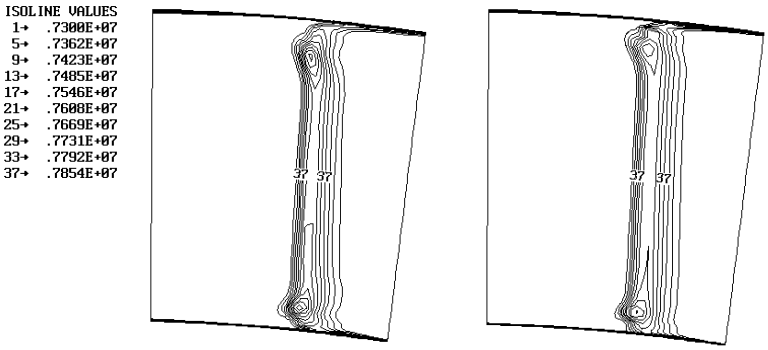

Fig. 9. HPT2 - total pressure contours downstream of the stator; Baldwin-Lomax (left), Menter SST (right).

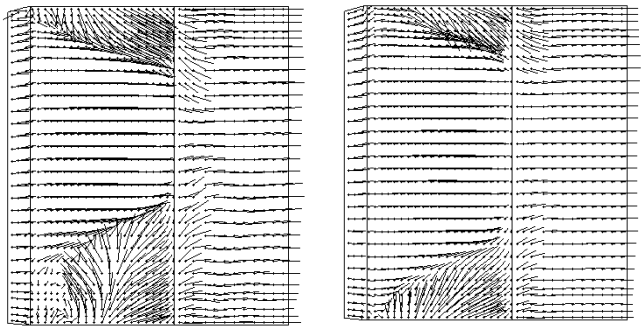

Fig. 10. HPT2 - velocity vectors at the suction surface of the rotor; Baldwin-Lomax (left), Menter SST (right).

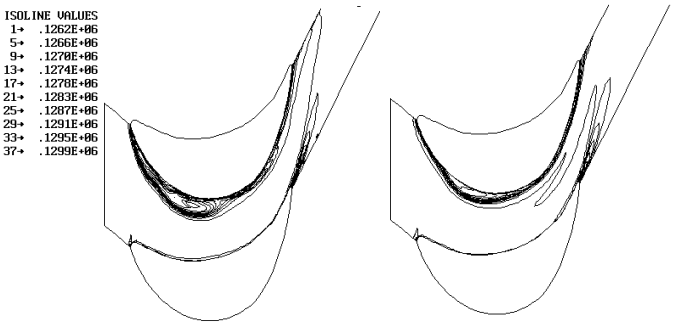

Fig. 11. HPT2 - entropy function contours in the rotor 6% blade span from root; Baldwin-Lomax (left), Menter SST (right).

Baldwin-Lomax model. Entropy function contours in the rotor at subsequent sections presented in Fig. 12 illustrate the development of secondary flow patterns and separation in the rotor, with the same tendency as observed in the stator that the loss centres due to secondary flows (at the root due to secondary flows and separation combined) remain closer to the endwalls, and the wake and boundary layers are slightly thicker in the Menter SST model.

Fig. 13 shows a span-wise distribution of kinetic energy losses in the stator, rotor and stage without the exit energy captured at the same distances downstream of the respective trailing edges as in the previous example. The tendency is that there is practically little difference in determination of the profile boundary layer losses between the two models. The Menter SST model predicts more eddy viscosity in the wake, secondary flow regions and separation zones. This results in more trailing edge loss, and also secondary loss and separation loss, say, per volume of the secondary flow and separation zones. However, the difference in secondary and separation losses between the two models is decreased due to a smaller extension of the secondary flow and separation zones in the Menter SST model. The secondary and separation loss maxima are considerably relocated, compared to those of the Baldwin-Lomax model. The pitch/span averaged value of the stator loss differs by 0.2% (BL - 3.1%, SST - 3.3%), the rotor loss - 0.6% (BL - 7.8%, SST - 8.4%), the stage loss without the exit energy differs again by 0.3% only (BL - 5.1%, SST - 5.4%). Although peaks of the rotor exit swirl angle in Fig. 14 undergo considerable changes in position and magnitude, the mean exit swirl angle practically does not change. For the same pressure drop, the resultant mass flow rate for the Baldwin-Lomax model is 165.5 kg/s, for Menter SST - 165 kg/s.

Although the flow in the stage HPT2 has a more complex nature, compared to that of the stage HPT1, mainly due to the interaction of the separation with the main flow and secondary flows, and there are significant redistributions of losses span-wise, the difference in pitch/span averaged values of the stage loss is still a mere 0.3%.

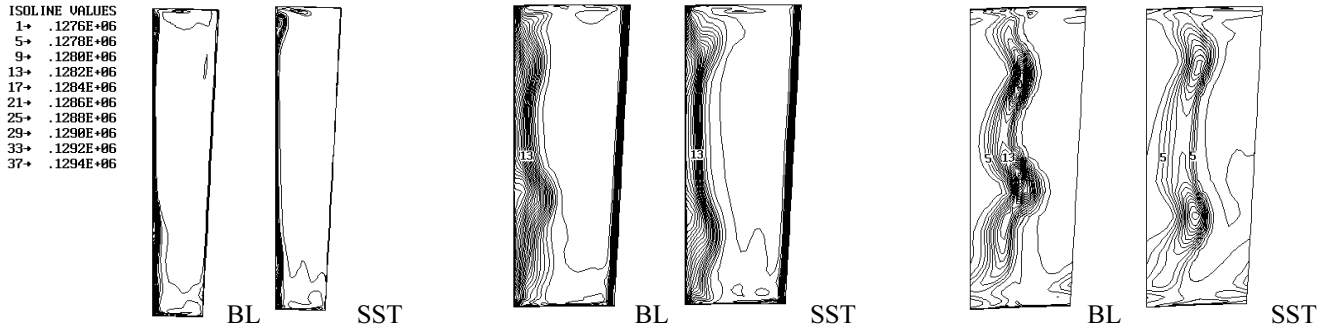

Fig. 12. HPT2 - entropy function contours in the rotor: 75% axial chord downstream of the leading edge (left), at the trailing edge (centre) and 18% axial chord downstream of the trailing edge (right); Baldwin-Lomax (left), Menter SST (right).

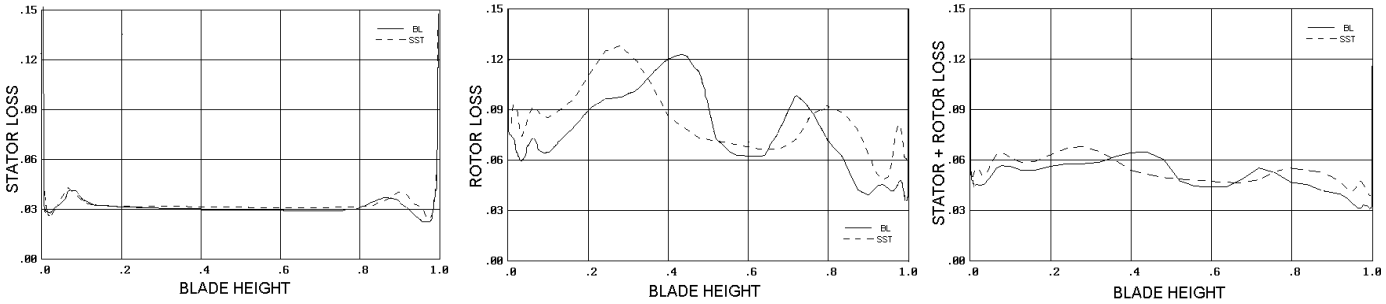

Fig. 13. HPT2 - span-wise distribution of kinetic energy losses in the stator (left), rotor (centre) and stage without exit energy (right).

Fig. 14. HPT2 - span-wise distribution of rotor exit swirl angle.

CONCLUSIONS

Two HP stator-rotor stages have been computed using a 3D RANS solver FlowER with closures in the form of the modified algebraic eddy-viscosity model of Baldwin-Lomax, or the two-equation eddy-viscosity shear stress transport model of Menter, a relatively new two-equation model combining good features of the k-ω and k-ε models. The computations show that the Menter SST model predicts more eddy viscosity in the wake, secondary flow regions and separation zones. However, a smaller extension of the secondary flow and separation zones is observed in the Menter SST model. There are alterations in span-wise distributions of kinetic energy losses in each blade row and the stage as a whole, by moving slightly up the 2D loss base (increased trailing edge loss), and increasing and relocating 3D peaks, which remain closer to the endwalls in the Menter SST model. There are also changes in the mean and span-wise distribution of the exit velocity and swirl angle. However, the pitch/span-averaged values of the overall stage loss do not significantly differ both for regular HP turbine flow patterns, and those more complex. Although the Menter SST model has an upper hand over the Baldwin-Lomax model in modelling transonic turbomachinery flows, especially compressor flows, the computations carried out for this paper also authorise the use of the less advanced Baldwin-Lomax model for engineering applications with regards to HP turbines.

REFERENCES

Baldwin B.S., Lomax H., 1978, Thin layer approximation and algebraic model for separated turbulent flows, *AIAA Paper,* No 78-257.

Chien K.Y., 1982, Predictions of channel and boundary-layer flows with a low-Reynolds number turbulence model, *AIAA J.,* Vol. 20, No. 1.

Chima R.V., 1996, A k-ω turbulence model for quasi-three-dimensional turbomachinery flows, *AIAA Paper,* No 96-0248.

Colantuoni S., Terlizzi A., Grasso F., 1989, A validation of a Navier-Stokes 2D solver for transonic turbine cascade flows, *AIAA Paper* No 2451.

Fletcher C.A.J., 1988, *Computational Techniques for Fluid Dynamics 2. Specific Techniques for Different Flow Categories*, Springer-Verlag Berlin, Heidelberg.

Johnson D.A., King L.S., 1985, Mathematically simple tur-

bulence closure model for attached and separated turbulent boundary layers, *AIAA J.,* Vol. 19, No. 11.

Jones W.P., Launder B.E., 1973, The calculation of low-Reynolds number phenomena with a two-equation model of turbulence, *Int. J. Heat and Mass Transfer*, Vol. 16, No. 10.

Kinsey D.W., Eastep F.E., 1988, Navier-Stokes solution for a thick supercritical airfoil with strong shocks and massively separated flow, *AAIA Paper,* No 0706.

Lampart P., Œwirydczuk J., Yershov A., Rusanov A., 2001, CFD analysis of 3D subsonic cascade flows (submitted for publication)

Larsson J., 1996, Numerical simulation of turbine blade heat transfer, *Licentiate of Engineering Thesis*, Chalmers University of Technology, Sweden.

Launder B.E., Sharma B.I., 1974, Application of energy-dissipation model of turbulence to the calculation of flow near a spinning disc, *Letters in Heat and Mass Transfer*, Vol. 1, No. 2.

Menter F.R., 1994, Two-equation eddy-viscosity turbulence models for engineering applications, *AIAA J.,* Vol. 32, No. 8.

Menter F.R., 1996, A comparison of some recent eddy-viscosity turbulence models, *Trans. ASME J. Fluids Engineering,* Vol. 118, No. 3.

Rody W., Srinivas K., 1989, Computation of flow and losses in transonic turbine cascades, *Z. Fluwiss. Weltraumforsch*, No 13.

Wiechowski S., 1988, Results of investigations of annular cascades TK8, TK9 and models TK8-TW3, TK9-TW3*, Rep. Institute of Thermal Engng £ódŸ* (in Polish).

Wilcox D.C., 1988, Reassessment of the scale-determining equation for advanced turbulence models, *AIAA J.,* Vol. 26, No. 11.

Wilcox D.C., 1993, Comparison of two-equation turbulence models for boundary layers with pressure gradient, *AIAA J.,* Vol. 31, No. 8.

Wilcox D.C., 1993, Turbulence modelling for CFD, DCW Industries Inc., La Canada, California.

Wilcox D.C., 1994, Simulation of transition with a two-equation turbulence model, *AIAA J.,* Vol. 32, No. 2.

Yershov S., Rusanov A., 1996a, The high resolution method of Godunov's type for 3D viscous flow calculations*, Proc. 3 Colloq. Proc. Simulation*, Espoo, Finland, June 13-16.

Yershov S., Rusanov A., 1996b, The application package FlowER for calculation of 3D viscous flows through multi-stage turbomachinery*, Certificate of Ukrainian state agency of copyright and related rights,* Kiev, Ukraine, February 19.

Yershov S., Rusanov A., 1997, Modification of algebraic turbulence model used in code FlowER, In Modelling Turbulence in Technical Applications*, Copybooks of Institute of Fluid-Flow Machinery*, No 486, Gdañsk, Poland.

Yershov S., Rusanov A., Gardzilewicz A., Lampart P, 1999, Calculations of 3D viscous compressible turbomachinery flows, *2nd Symp. on Comp. Technologies for Fluid/Thermal/ Chemical Systems with Industrial Applications, ASME PVP Division Conf.,* August 1-5, Boston, USA, *ASME PVP* - Vol. 397, No. 2.

Yershov S., Rusanov A., Shapochka A., 2001, 3D viscous transonic turbomachinery flows: Numerical simulation and optimisation using code FlowER, *Proc. Conf. V ISAIF'2001*, September 4-7, Gdañsk, Poland (to appear).

APPENDIX

In this chapter, kinetic energy losses in the stator, rotor and stage are defined. Fig. A1, which illustrates the process of expansion in a turbine stage in the form of an enthalpy-entropy diagram, will help to explain definitions gathered in Tab. A1.

Stator loss	$\xi_1 = (h_1 - h_{1s}) / (h_{0T} - h_{1s})$
Rotor loss	$\xi_2 = (h_2 - h_{2s}) / (h_{1T} - h_{2s})$
stage loss without exit energy = stator + rotor loss	$\xi_{12} = (h_2 - h_{2s'}) / (h_{0T} - h_{2s'})$
stage loss with exit energy	$\xi_{12c} = (h_{2T} - h_{2s'}) / (h_{0T} - h_{2s'})$

Tab. A1. Kinetic energy losses in the stator, rotor and stage.

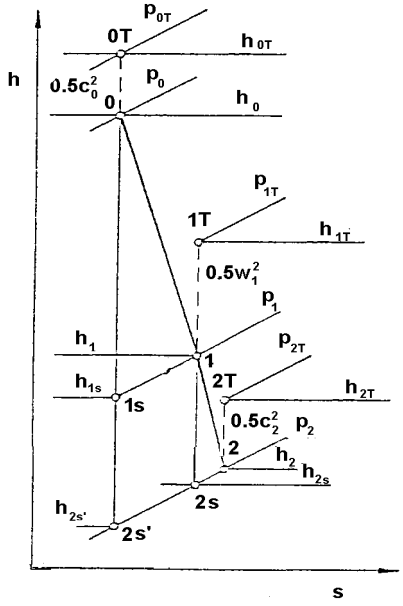

Symbols:

c - absolute velocity,
h - enthalpy,
p - pressure,
s - entropy,
w - relative velocity,

Subscripts:

0 - inlet
1 - behind the stator
2 - behind the stage
s, s' - isentropic
T - total

Fig. A1. Enthalpy-entropy diagram for a turbine stage.